






Trophic state alters the mechanism whereby energetic coupling between photosynthesis and respiration occurs in *Euglena gracilis*

Gwenaëlle Gain^{1*} , Félix Vega de Luna^{1*}, Javier Cordoba¹, Emilie Perez¹, Hervé Degand², Pierre Morsomme² , Marc Thiry³, Denis Baurain⁴ , Mattia Pierangelini^{1†}  and Pierre Cardol^{1†} 

¹InBioS – PhytoSYSTEMS, Laboratoire de Génétique et Physiologie des Microalgues, ULiège, Liège B-4000, Belgium; ²Louvain Institute of Biomolecular Science and Technology (LIBST), UCLouvain, Louvain-la-Neuve B-1348, Belgium; ³Laboratoire de Biologie Cellulaire et Tissulaire, Giga-Neurosciences, ULiège, Liège B-4000, Belgium; ⁴InBioS – PhytoSYSTEMS, Eukaryotic Phylogenomics, ULiège, Liège B-4000, Belgium

Summary

Author for correspondence:
Pierre Cardol
Email: pierre.cardol@uliege.be

Received: 4 May 2021
Accepted: 6 August 2021

New Phytologist (2021)
doi: 10.1111/nph.17677

Key words: bioenergetics, *Euglena*, metabolism, mixotrophy, organelle interaction, photoautotrophy.

- The coupling between mitochondrial respiration and photosynthesis plays an important role in the energetic physiology of green plants and some secondary-red photosynthetic eukaryotes (diatoms), allowing an efficient CO₂ assimilation and optimal growth.
- Using the flagellate *Euglena gracilis*, we first tested if photosynthesis–respiration coupling occurs in this species harbouring secondary green plastids (i.e. originated from an endosymbiosis between a green alga and a phagotrophic euglenozoan). Second, we tested how the trophic state (mixotrophy and photoautotrophy) of the cell alters the mechanisms involved in the photosynthesis–respiration coupling.
- Energetic coupling between photosynthesis and respiration was determined by testing the effect of respiratory inhibitors on photosynthesis, and measuring the simultaneous variation of photosynthesis and respiration rates as a function of temperature (i.e. thermal response curves). The mechanism involved in the photosynthesis–respiration coupling was assessed by combining proteomics, biophysical and cytological analyses.
- Our work shows that there is photosynthesis–respiration coupling and membrane contacts between mitochondria and chloroplasts in *E. gracilis*. However, whereas in mixotrophy adjustment of the chloroplast ATP/NADPH ratio drives the interaction, in photoautotrophy the coupling is conditioned by CO₂ limitation and photorespiration. This indicates that maintenance of photosynthesis–respiration coupling, through plastic metabolic responses, is key to *E. gracilis* functioning under changing environmental conditions.

Introduction

In photosynthetic organisms, it is a commonly accepted view that the ATP/NADPH ratio generated by photosynthetic linear electron flow is insufficient to sustain CO₂ import into the plastid and assimilation by the Calvin–Benson–Bassham cycle (Allen, 2002; Allen *et al.*, 2008; Bailleul *et al.*, 2015). In this respect, the activities of several plastid-localized alternative electron pathways (AEPs) contribute to establishing the proton motive force necessary to produce additional ATP without net NADPH generation. These AEPs include cyclic electron flow around photosystem II (PSII) (Feikema *et al.*, 2006) or around photosystem I (PSI) and the water-to-water cycles (i.e. flavodiiron proteins, Mehler-ascorbate peroxidase, plastoquinol terminal oxidase, oxygenase activity of RuBisCO (photorespiration)) that mediate electron

flow from oxidation of water to reduction of O₂ (Cardol *et al.*, 2011; McDonald *et al.*, 2011; Raven *et al.*, 2020).

Besides AEPs localized in the chloroplasts, optimization of ATP/NADPH budget can also rely on the sharing and rerouting of ATP and NADPH between chloroplasts and mitochondria. This has been shown in several species of photosynthetic eukaryotes, including flowering plants (Raghavendra & Padmasree, 2003; Noguchi & Yoshida, 2008), primary green algae (*Chlamydomonas reinhardtii*; Cardol *et al.*, 2003; Dang *et al.*, 2014) and complex algae bearing plastids of red origin such as the diatom *Phaeodactylum tricornutum* (Bailleul *et al.*, 2015; Murik *et al.*, 2019) or the dinoflagellate *Symbiodinium* sp. (Pierangelini *et al.*, 2020). It thus appears that the energetic chloroplast–mitochondrion coupling occurs in microalgal species with different evolutionary origins or from different ecological niches.

Euglena gracilis (Euglenozoa, Discoba, Excavata) is a unicellular photosynthetic eukaryote originating from an endosymbiosis

*These authors contributed equally to this work.

†These authors share senior authorship.

between a green alga (Pyramimonadales) and an ancient phagotrophic euglenozoan species (Turmel *et al.*, 2009; Jackson *et al.*, 2018). Lateral gene transfer events from other microorganisms (Novák Vanclová *et al.*, 2020) enriched the evolutionary history of Euglenoids with respect to the 'green' and 'red' primary algae. Because of this, *E. gracilis* has become increasingly relevant to understanding the changes that the 'green' secondary endosymbiosis has caused to both chloroplastic metabolism (Bennett *et al.*, 2012; Novák Vanclová *et al.*, 2020) and mitochondrial machinery (Perez *et al.*, 2014; Yadav *et al.*, 2017; Hammond *et al.*, 2020). *Euglena gracilis* chloroplast has three envelope membranes (Larkum *et al.*, 2007) and a reticulated mitochondrial network (Pellegrini, 1980). In relation to the respiratory apparatus, additional atypical domains have been found in complex I (CI) and complex IV (CIV) of the respiratory electron transport chain (Miranda-Astudillo *et al.*, 2018), and the Krebs cycle has an alternative pathway from 2-oxoglutarate to succinate (via 2-oxoglutarate decarboxylase) (Raven & Beardall, 2016). In the chloroplast, Shimakawa *et al.* (2017) suggested the possible presence of two (or more) AEP mechanisms, including an AEP with low affinity for O₂ (e.g. photorespiration). Yet, it is still not known whether, during evolution, *E. gracilis* retained the mechanisms connecting photosynthetic activity to respiration (e.g. NADPH and ATP exchange). The primary aim of our work is thus to investigate the chloroplast–mitochondrion energetic coupling in *E. gracilis*, thereby expanding on the role of chloroplast–mitochondrion coupling in regulating the cell ATP/NADPH budget in phylogenetically distant species (Wilken *et al.*, 2014), and thus on its possible multiple and independent appearances.

In addition to its key evolutionary history, *E. gracilis* represents an interesting model related to its ability to grow in the presence of both inorganic carbon (C_i) and organic carbon sources (e.g. acetate, ethanol) (Perez *et al.*, 2014). The presence of organic substrates promotes mixotrophic growth and may reduce the need for an active photosynthetic apparatus (Chapman *et al.*, 2015), for example, involving less pigments, RuBisCO, PSII or PSI biosynthesis (Wilken *et al.*, 2014; Kamalanathan *et al.*, 2017; Cecchin *et al.*, 2018), or a CO₂-concentrating mechanism activity (Polukhina *et al.*, 2016; Treves *et al.*, 2016). This shifts the role of photosynthesis from providing both carbon and energy to mainly providing energy (Wilken *et al.*, 2014). Contemporaneously to these alterations, organic substrates stimulate cell respiration (Perez *et al.*, 2014), potentially altering the mechanisms whereby the mitochondria interact with the chloroplasts. Our second aim is thus to determine how the cell trophic state influences the coupling and the exchange of metabolites between chloroplasts and mitochondria in *E. gracilis*.

Materials and Methods

Strain and culture conditions

Euglena gracilis strain (SAG 1224-5/25, obtained from the University of Göttingen (Sammlung von Algenkulturen, Germany), was grown under low photosynthetic photon flux density

(PPFD) (LL, 50 μmol photons m⁻² s⁻¹, white light-emitting diode (LED)) at 25°C in Tris-minimal-phosphate (TMP) liquid medium (Perez *et al.*, 2014). Unless specified, TMP + LL was chosen to set the photoautotrophic condition, whereas TMP added to acetate (17 mM) as an exogenous organic carbon source (i.e. Tris-acetate-phosphate, TAP) was chosen as the mixotrophic condition. The effects of different carbon sources (60 mM acetate, 22–220 mM ethanol, in combination with darkness or moderate PPFD (ML, 200 μmol photons m⁻² s⁻¹), were tested after 48 h after their addition to TMP cells grown in LL. All media were supplemented with vitamins (biotin, 10⁻⁷%; vitamin B12, 10⁻⁷%; vitamin B1, 2 × 10⁻⁵% (w/v); Perez *et al.*, 2014). For each experiment, cell concentration was determined with a Beckman Coulter Z2 Counter Analyser (Z2; Beckman, Indianapolis, IN, USA).

Oxygen exchange measurements

Rates of photosynthesis and dark respiration (R_d) were measured on exponentially growing cells using a Clark-type oxygen electrode (Hansatech, King's Lynn, UK). Briefly, cells were harvested from the culture by centrifugation (3500 g, 2 min), resuspended in fresh culture medium (TAP or TMP), and placed into the oxygen electrode chamber. For each measurement, temperature was kept at 25 ± 1°C. For cells grown photoautotrophically, 2 or 10 mM of NaHCO₃ was added during the experiment to guarantee a sufficient supply of C_i (Iglesias-Prieto *et al.*, 1992; Karsten & Holzinger, 2012). Respiration rates were measured after 5–10 min in the dark. Photosynthesis was measured under a red light source (provided by LED peaking at 660 nm; see figure legends for each PPFD and duration). Gross oxygen production (E_O) was calculated as the difference between net photosynthesis and R_d . To test the impact of respiratory inhibitors on photosynthesis, inhibitors of mitochondrial complexes were added at the beginning of the measurements. These included oligomycin (50 μM, blocking mitochondrial F₁F₀ ATP synthase), antimycin A (AA, 10 μM, blocking CIII), rotenone (100 μM, blocking CI), potassium cyanide (KCN, 1 mM, blocking CIV) and salicylhydroxamic acid (SHAM, 1 mM, blocking mitochondrial alternative oxidase (AOX)) (Perez *et al.*, 2014). Stock solutions of oligomycin, AA, rotenone and SHAM were prepared in dimethyl sulfoxide. Stock solution of KCN was prepared in deionized water. Aminoxyacetic acid (AOAA, O-(carboxymethyl) hydroxylamine hemihydrochloride, 5 mM) was also used as an inhibitor of the aspartate aminotransferase (Cornell *et al.*, 1984) involved in the malate-aspartate shuttle. Aminoxyacetic acid was added to cells maintained in darkness for 2 min before measurements.

Thermal response curves (TRCs) were carried out as in Karsten & Holzinger (2012) and Pierangelini *et al.* (2020). *Euglena gracilis* was exposed to rising temperatures from 10 to 40°C. At each temperature, cells were initially incubated in the dark for 25 min, and the last 10 min of this incubation period was used to measure R_d . After the dark period, cells were exposed to a PPFD of 400 μmol photons m⁻² s⁻¹ (LED light source peaking at 660 nm) for 10 min, with the final 5 min used to calculate $E_{O,max}$.

Growth

To determine the growth of *E. gracilis* under mixotrophic and photoautotrophic conditions in the absence or presence of respiratory inhibitors (rotenone (100 μM) and AA (10 μM)), batch cultures (25 ml of medium in a flask of 100 ml) were started with exponentially growing cells, at an initial cell concentration $\leq 4 \times 10^4$ cells ml^{-1} . Cell concentration was measured daily until the end of the exponential phase. Cell-specific division rate (μ) was calculated from the slope of the natural logarithm plot obtained from the exponential phase of the growth curve.

Spectroscopic measurements

Chlorophyll content Cells were harvested by centrifugation (2500 g , 1 min) and resuspended in cold 100% methanol. This suspension was then centrifuged (2500 g , 1 min) and the absorbance of the supernatant measured in a spectrophotometer (Lambda 265; Perkin Elmer, Waltham, MA, USA) at 665 and 652 nm. Total Chl(*a* + *b*) concentration was calculated using equations for chlorophytes from Ritchie (2006). When needed, cells were resuspended in medium supplemented with ficoll 10% to a final Chl concentration of 10 $\mu\text{g ml}^{-1}$, and were dark-acclimated for at least 20 min with constant stirring.

Electrochromic shift The development of the light-induced thylakoid electric field ($\Delta\psi$) was followed *in vivo* by monitoring changes in absorption of membrane-embedded pigments (commonly referred to as electrochromic shift; ECS) (Bailleul *et al.*, 2010). Measurements were carried out with a Joliot-Type Spectrophotometer (JTS-10; Biologic, Seyssinet-Pariset, France) equipped with a white probing LED and interference filters (10 nm bandwidth). The ECS signal was recorded within the 440–600 nm region as the changes of absorption from a baseline in the darkness to the signal 150 μs after applying a saturating single turnover flash (duration *c.* 7 ns; Nd-YAG laser Minilite II, Continuum, Milpitas, CA, USA). The ECS spectrum response was similar for *E. gracilis* cells grown mixotrophically and photoautotrophically (Supporting Information Fig. S1a), with a maximum at 510 nm. The ECS at 510 nm was used to monitor the linearity of the signal increase (Fig. S1b) and the maximum electric field generated by a series of charge separations induced by the laser flash fired each 100 ms until the maximum signal was reached. When used, the mitochondrial respiratory inhibitors KCN (1 mM) and SHAM (1 mM) were added 1 min before measurements. The presence of mitochondrial inhibitors had only a minor effect on the signal increase corresponding to one charge separation ($92 \pm 4\%$ and $85 \pm 5\%$ of the control values in photoautotrophic and mixotrophic conditions, respectively).

Chl*a* fluorescence Measurements were carried out in the JTS-10 spectrophotometer with a detecting probe providing short blue flashes (10 μs duration, 440–470 nm) and fluorescence was recorded after light was filtered by a long-pass filter (680 nm). Actinic light was provided by red LEDs (660 nm) either as a saturating pulse (9000 $\mu\text{mol photons m}^{-2} \text{s}^{-1}$ during 150 ms) or as

continuous illumination to maintain steady photosynthesis. The potential direct effect of inhibitors on photosynthetic electron transfer was monitored during the Chl fluorescence increase as a result of strong illumination (2750 $\mu\text{mol photons m}^{-2} \text{s}^{-1}$) during 500 ms followed by a 150 ms saturating pulse. Each inhibitor tested was added less than 2 min before the measurements to TAP or TMP dark-acclimated cells (Fig. S2). The impact of DCMU (3-(3,4-dichlorophenyl)-1,1-dimethylurea, 10 μM , prepared in methanol), and DBIMB (2,5-Dibromo-6-isopropyl-3-methyl-1,4-benzoquinone, 5 μM , prepared in ethanol) were evaluated as controls (Fig. S2).

Post-illumination Chl fluorescence recordings were obtained after 12 min of light acclimation in the JTS-10 (100 $\mu\text{mol photons m}^{-2} \text{s}^{-1}$) with constant stirring. Rotenone (100 μM), AOAA (5 mM) or sodium bicarbonate (10 mM) were added at the fourth minute of the light phase followed by the addition (or the absence in the case of control measurement) of octyl gallate (OG, 10 μM , prepared in dimethyl sulfoxide), blocking the plastidial terminal oxidase (PTOX). The changes of Chl fluorescence between 5 and 60 s of the post-illumination phase were calculated after normalization of the fluorescence traces by setting F_0 to 1. At the end of the light phase, the nonphotochemical quenching of Chl fluorescence (NPQ, calculated as $(F_m - F_m')/F_m'$, where F_m is the maximum fluorescence of cells before illumination and F_m' is the maximum fluorescence before light is switched off) were very low and identical in the presence or absence of OG in mixotrophy or in photoautotrophy (Fig. S3) (two-way ANOVA; $P > 0.1$) so the contribution of NPQ relaxation to F_0 changes (if any) should be negligible. Relative electron transport rate through PSII (rETR-PSII, $\mu\text{mol electrons m}^{-2} \text{s}^{-1}$) was calculated as $\text{PPFD} \times (F_m' - F_s)/F_m'$, where F_s is the steady-state fluorescence of cells in the light.

Transmission electron microscopy (TEM)

In addition to the standard mixotrophic and photoautotrophic conditions under low light, *E. gracilis* cells were grown in photoautotrophy + 5% CO_2 : 95% air mixture bubbled in the culture. Cells were fixed for 60 min at room temperature in 2.5% glutaraldehyde in 0.1 M Sorensen's buffer (pH 7.4). After washing in Sorensen's buffer, cells were postfixed in 2% osmium tetroxide (CAS: 20816-12-0), dehydrated through graded ethanol-propylene oxide series and embedded in epoxy resin (SPI-PON 812; Spichem, West Chester, PA, USA). The resin was then polymerized at 60°C for 48 h. Ultrathin sections (80 nm) were mounted on colloidin-coated grids and stained with uranyl acetate and lead citrate before examination in a JEM 1400 transmission electron microscope at 80 kV.

Statistical analyses

Experiments were performed with at least three (unless otherwise stated) biological replicates. Comparisons between two treatments were made using two-tailed *t*-tests. When comparison involved more than two treatments, one-way ANOVA was used. Changes of parameters as a function of increasing temperature or

changes during exposure to respiratory inhibitors were tested using repeated-measures (RM) ANOVA. The variation among means in relation to treatments was tested by using two-way ANOVA. The analyses were performed using GRAPHPAD PRISM 5 (GraphPad Software, San Diego, CA, USA), setting the threshold of significance at 0.05.

Comparative proteomics

Preparation of protein samples In addition to the standard mixotrophic and photoautotrophic conditions under low light, we analysed mixotrophic cells under moderate light (TAP ML) and photoautotrophic cells in the presence of the 5% CO₂ : 95% air mixture bubbled in the culture (TMP CO₂). The membrane and soluble proteins were obtained as outlined in Remacle *et al.* (2006). All steps were performed at 4°C. Briefly, 20 µg of proteins (quantified by the Bradford assay (Bradford, 1976)) from each sample were precipitated in cold chloroform-methanol (Wessel & Flügge, 1984). Each sample was transferred to a 1.5 ml tube and adjusted to 100 µl with H₂O. Chloroform (100 µl) and methanol (400 µl) were added and the mixture vortexed for 30 s. Samples were then added with 300 µl of H₂O and the mixture was vortexed again for 30 s. Each sample was then centrifuged (4°C, 20 000 g, 15 min) and after removing the upper phase, 800 µl of methanol was added. The samples were then re-centrifuged (4°C, 20 000 g, 15 min), and the protein pellet vacuum-dried (SC 200 Savant Speed Vac Concentrator; ThermoFisher Scientific, Waltham, MA, USA) and then stored at -20°C. Before analysis, proteins were trypsin-digested according to Szopinska *et al.* (2011).

Shotgun proteomics and protein quantification Full details of this procedure, including comments about the total number of proteins identified, are given in Methods S1 and other supplementary materials. The relative abundance of proteins in each condition was determined using iTRAQ isobaric labelling. The iTRAQ marking was carried out according to the protocol supplied by the manufacturer (AB Sciex, Foster City, CA, USA). After isobaric labelling, the four samples were mixed and the mixture dried under vacuum in an SC 200 Savant Speed Vac concentrator. Sixteen micrograms of proteins for each labelled sample were then dissolved in 0.025% trifluoroacetic acid and 5% acetonitrile and subjected to reverse phase chromatography according to Szopinska *et al.* (2011), using an LC Ultimate nanochromatography system 3000 (ThermoFisher Scientific). The eluted peptides were analysed using an AB Sciex 4800 matrix-assisted laser desorption/ionization-time of flight MS as described in Szopinska *et al.* (2011). Each sample was analysed in three repetitions.

Peptides and proteins were inferred from the spectrum identification results using PEPTIDESHAKE v.1.16.43 (Vaudel *et al.*, 2015). Spectrum counting abundance indexes were estimated using the normalized spectrum abundance factor (Powell *et al.*, 2004) adapted for better handling of protein inference issues and peptide detectability. Finally, protein quantification was performed with REPORTER v.0.7.20 (beta). Normalized protein

abundance was then log₂-transformed and significant changes ($P < 0.05$) between samples were computed using a linear model framework with LIMMA empirical Bayes approach (Kammers *et al.*, 2015; Ritchie *et al.*, 2015).

Results and Discussion

Mixotrophy increases the $R_d : E_{O,max}$ ratio

We compared dark respiration (R_d) to maximal gross oxygen evolution (E_O) of *E. gracilis* growing in the presence and absence of organic substrates. The total Chl concentration was 15.9 ± 1.8 pg per cell in mixotrophy with no significant difference with respect to cells in photoautotrophy (18.3 ± 4.3 pg Chl per cell; one-way ANOVA, $P = 0.20$) (Table 1), allowing us to express any metabolic activity on a cell or a Chl basis. In mixotrophy, the $R_d : E_{O,max}$ ratio for *E. gracilis* was significantly higher than in photoautotrophy (0.40 ± 0.03 ; one-way ANOVA, $P = 0.01$), probably because of the involvement of R_d in heterotrophic metabolism to provide the energy for biosynthesis (Geider & Osborne, 1989). These $R_d : E_{O,max}$ ratios in *E. gracilis* are in the range of values (0.1–0.5) previously reported for other microalgal species (Geider & Osborne, 1989; Raven & Beardall, 2016; Pierangelini *et al.*, 2019). We then investigated whether a sudden change in respiratory capacity was reflected by a change of photosynthesis in *E. gracilis*.

Reduction in photosynthetic performance following inhibition of mitochondrial respiration

We evaluated the impact of inhibition of the mitochondrial respiratory complexes (I, III and IV), mitochondrial AOX, and mitochondrial F₁F₀ ATP synthase on R_d and E_O . In mixotrophy, addition of rotenone (blocking complex I), AA (blocking complex III), KCN (blocking complex IV), KCN + SHAM (blocking complex IV and AOX, respectively), or oligomycin (blocking mitochondrial F₁F₀ ATP synthase) caused significant reductions in R_d (50%, 71%, 91%, 91%, 67%, respectively) (Fig. 1a), similar to those previously reported by Perez *et al.* (2014). The absence of effect of SHAM addition (Fig. 1a) or octyl gallate (Fig. S4) on KCN-resistant R_d indicated that the apparent capacity of AOX (SHAM-sensitive rate) is null or extremely low as previously reported (Castro-Guerrero *et al.*, 2004; Perez *et al.*, 2014; Krnáčová *et al.*, 2015). Conversely, the large KCN-sensitive respiration indicated a high capacity of the CIII + CIV pathway in mixotrophic conditions. In photoautotrophy, addition of rotenone and AA caused a 30–40% decline in R_d . Addition of every inhibitor (except SHAM) caused a significant decrease in $E_{O,max}$ (Fig. 1a). In mixotrophy, the $R_d : E_{O,max}$ ratio was not altered by the presence of rotenone, oligomycin, KCN or SHAM, reflecting the fact that the extent of the inhibition of $E_{O,max}$ was proportional to the inhibition of R_d (Fig. 1b). This ratio was, however, lower in presence of AA and KCN + SHAM as a result of a lesser inhibition of $E_{O,max}$ than R_d . In photoautotrophy, the $R_d : E_{O,max}$ ratio decreased by 20% (Fig. 1b). For cells in both trophic conditions, a linear relationship ($r^2 = 0.90$, $P = 0.0003$)

Table 1 Parameters extrapolated from the transmission electron micrographs of *Euglena gracilis* cells cultured in mixotrophy, photoautotrophy and photoautotrophy + 5% CO₂ (Figs 8, S7).

	Mixotrophy	Photoautotrophy	Photoautotrophy + 5% CO ₂
Chl content (pg per cell)	15.9 (1.8) ^a	18.3 (4.3) ^a	20.5 (4.6) ^a
Cell length (μm)	13.8 (2.5) ^a	14.6 (2.6) ^a	14.2 (5.2) ^a
Mitochondrial section area (μm ²)	0.2 (0.04) ^a	0.3 (0.08) ^a	0.3 (0.07) ^a
Number of mitochondrial sections per cell	14.2 (4.3) ^a	7.7 (2.4) ^b	8.2 (5.7) ^b
Chloroplast section area (μm ²)	1.8 (0.6) ^a	3.4 (1.7) ^{ab}	3.7 (0.6) ^b
Number of chloroplast section per cell	4.5 (1.4) ^a	5.9 (3.7) ^a	7.6 (3.8) ^a
Chloroplast/mitochondria total area ratio	3.0 (1.4) ^a	8.2 (3.0) ^b	9.6 (4.0) ^b
Mitochondrial sections in contact with chloroplast contact (%)	58 (25) ^a	78 (16) ^a	74 (16) ^a
Membrane contact sites length (μm)	0.50 (0.12) ^a	0.43 (0.10) ^a	0.55 (0.13) ^a
Pyrenoid/chloroplast section area	0.04 (0.03) ^a	0.07 (0.04) ^a	0.03 (0.01) ^a
Number of intrapyrenoid thylakoids	4.5 (0.5) ^a	3.4 (2.5) ^a	6.3 (3.6) ^a

Values in brackets represent SD. Different letters identify significantly different means (one-way ANOVA, $P < 0.05$) among treatments.

was found between the reduction of R_d and $E_{O,max}$ caused by the addition of respiratory inhibitors (Fig. 1c). Because there is no direct immediate effect of these inhibitors on Chl a fluorescence induction curves (Fig. S2), the inhibition of $E_{O,max}$ thus resulted from indirect effects, very likely caused by direct inhibition of mitochondrial respiration. E_O was also measured at sub-saturating light intensities, and the general trends were similar (Fig. S5). However, differences in the extent of R_d and E_O inhibition between light intensities were observed (see legend text of Fig. S5 for details), and they might indicate the occurrence of either some compensatory/alternative pathways or various non-specific inhibitory effects (Roberty *et al.*, 2014). In two distant species, the diatom *P. tricornutum* and the green alga *C. reinhardtii*, the photosynthetic electron transfer rate also linearly followed changes in respiration upon inhibition of mitochondrial respiration (Cardol *et al.*, 2003; Bailleul *et al.*, 2015). In both species, the AOX has been identified as an electron sink for photosynthetic-reducing equivalents (Bailleul *et al.*, 2015; Kaye *et al.*, 2019). In *E. gracilis*, the apparent null capacity of AOX in mixotrophy (see earlier), but also in photoautotrophy (Fig. S5), rather suggests a strong dependence of photosynthetic electron transfer chain on mitochondrial respiratory electron flow coupled to ATP synthesis.

Similar changes of photosynthesis and respiration during rapid temperature exposure

In the next step, we tested the effect of rapid changes in temperature (from 10 to 40°C) on respiratory and photosynthetic capacities. We observed an overall similar increase of $E_{O,max}$ and R_d with temperature, whether cells were grown mixotrophically or photoautotrophically (e.g. about five times between 10°C and 35°C; t -test, $P < 0.01$) (Fig. 2a,b). This increase reflects the temperature sensitivity of electron-transport components and enzymatic machinery involved in both metabolic processes (Berry & Björkman, 1980; Atkin & Tjoelker, 2003). In agreement with the results reported in Fig. 1(b), the $R_d : E_{O,max}$ ratio for *E. gracilis* growing photoautotrophically was lower than for cells growing mixotrophically (Fig. 2c). These $R_d : E_{O,max}$ ratios were stable

from 10 to 35°C (one-way ANOVA; mixotrophy, $P = 0.67$; photoautotrophy, $P = 0.98$), which reflects the fact that both $E_{O,max}$ and R_d were equally sensitive to the increase of temperature, and indicative of a coupling between respiration and photosynthesis. By contrast, dissimilar temperature-dependent increases of photosynthesis and respiration (varying $R_d : E_{O,max}$) were observed in several other species of green algae (Padfield *et al.*, 2016; Schaum *et al.*, 2017; Pierangelini *et al.*, 2019), diatoms (Prelle *et al.*, 2019) and dinoflagellates (Pierangelini *et al.*, 2020), and these are an indication that photosynthesis may be less dependent on R_d in those species (Pierangelini *et al.*, 2020). Finally, in *E. gracilis*, the increase in $R_d : E_{O,max}$ at the high temperature tested (40°C) (Fig. 2c) could reflect the disruption of the photosynthesis–respiration coupling as a result of thermal stress, as was previously observed in dinoflagellates (Pierangelini *et al.*, 2020).

Parallel photosynthetic and respiratory capacities under different mixotrophic conditions

We then exposed photoautotrophic *E. gracilis* cells to changes in trophic conditions by modifying the light regime or adding an exogenous organic carbon source. Rates of R_d and E_O were measured after 36 h and are reported in Fig. 3(a). The presence and availability of different organic substrates (acetate or ethanol) caused a two- to 12-fold increase in the rates of R_d and E_O , in comparison to cells grown in photoautotrophic conditions. In agreement with the results reported in Fig. 1(c) for the $R_d : E_{O,max}$, the $R_d : E_O$ for cells growing mixotrophically was higher than that for cells growing photoautotrophically (Fig. 3b). Interestingly, despite the large changes in the rates of R_d and E_O , the $R_d : E_O$ ratio was similar under different organic substrates (one-way ANOVA, $P = 0.38$). This result again suggested that the coupling of the chloroplast with the mitochondrion is essential and has to be maintained regardless of the trophic conditions, to guarantee cell photosynthetic functioning. In relation to growth, in mixotrophy, addition of rotenone and AA caused *c.* 15% and 40% reductions of μ , respectively. When *E. gracilis* was grown photoautotrophically, μ was reduced *c.* 10% and 20% with rotenone and AA, respectively (Fig. S6). This μ reduction reflects

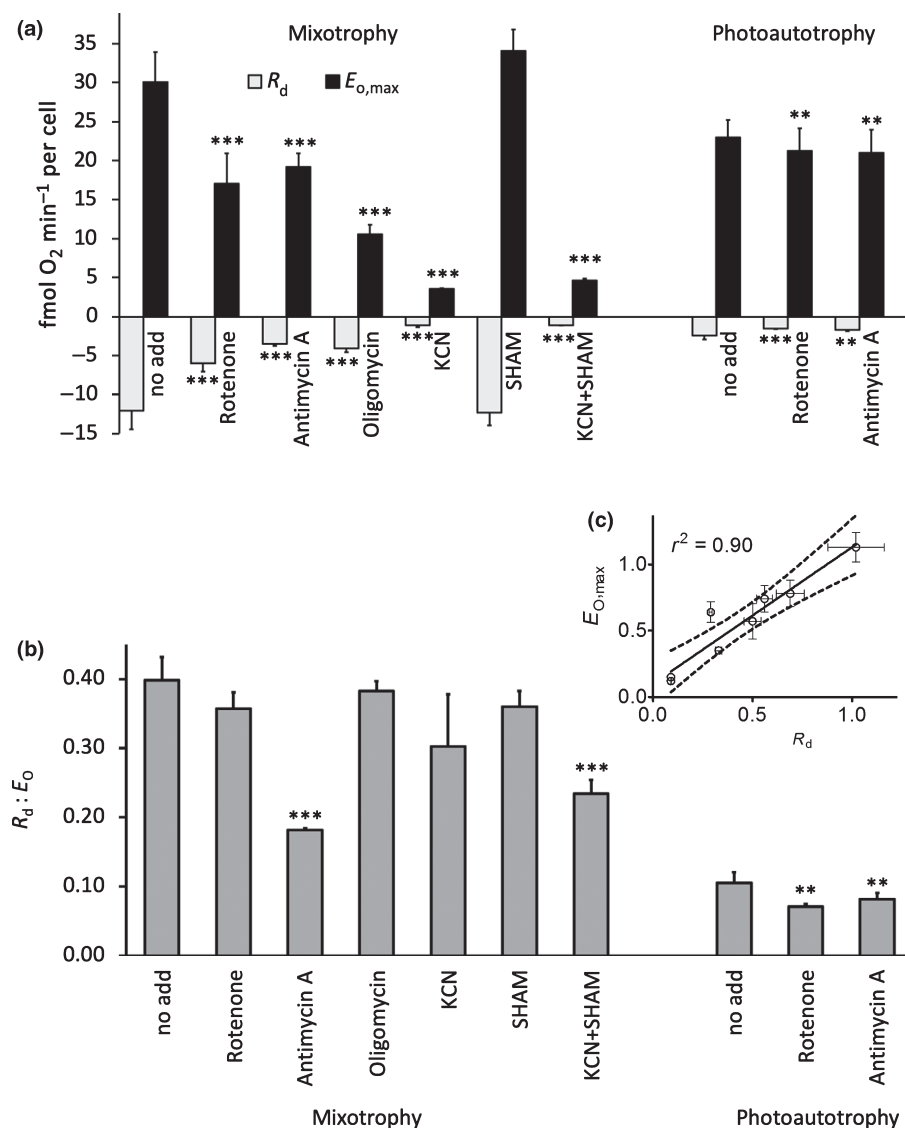


Fig. 1 Impact of mitochondrial respiratory inhibitors on dark respiration (R_d), gross maximal photosynthesis ($E_{O,\max}$) (a), and $R_d : E_{O,\max}$ ratios (b) in *Euglena gracilis* cultivated in mixotrophic and photoautotrophic conditions. All measurements were conducted in the presence of 10 mM NaHCO_3 . A total of 10^6 cells ml^{-1} were adjusted in the oximeter chamber. Each light step (30, 103, and $571 \mu\text{mol photons m}^{-2} \text{ s}^{-1}$) was held for 5 min. Vertical bars indicate the standard deviation. **, $P < 0.05$; ***, $P < 0.01$; Student's t -test (values were compared with the $E_{O,\max}$ or R_d values of noninhibited cells (no add)). (c) Linear relationship ($r^2 = 0.90$, $P = 0.0003$) between $E_{O,\max}$ and R_d in the presence of mitochondrial respiratory inhibitors for *E. gracilis* cultivated in mixotrophic and photoautotrophic conditions. All values were normalized to $E_{O,\max}$ and R_d values in the absence of inhibitors. Vertical and horizontal bars indicate the standard deviation.

the involvement of the respiratory metabolism in the production (from carbohydrates produced during photosynthesis) of cellular metabolites used in the construction of cells (Falkowski *et al.*, 1985; Geider & Osborne, 1989).

Exchange of energy currency compounds between chloroplasts and mitochondria

As the interdependence between respiratory and photosynthetic activities often involves an energetic exchange between chloroplasts and mitochondria (Cardol *et al.*, 2009; Bailleul *et al.*, 2015), we determined whether ATP of mitochondrial origin could be imported into the chloroplasts. For dark-acclimated *E. gracilis* cells in both mixotrophic and photoautotrophic conditions, the maximum trans-thylakoid electric field ($\Delta\psi$, that can be built under a 10 Hz single-turnover flash train) was about 5 r.u. (threshold value corresponding to a membrane potential reference (Joliot & Joliot, 2008)). In the presence of mitochondrial inhibitors (AA or KCN+SHAM), $\Delta\psi$ increased to *c.* 6 and 8 r.u., respectively

(Fig. 4a). This indicated that the $\Delta\psi$ obtained in the absence of inhibitors was superimposed on a $\Delta\psi$ component present in the dark ($\Delta\psi_{\text{dark}}$, *c.* up to 3 r.u.), which is disrupted following the inhibition of mitochondrial respiratory electron transfer chain. In flowering plants and diatoms, it was proposed that the $\Delta\psi_{\text{dark}}$ was the result of hydrolysis of ATP imported from mitochondria by the chloroplastic ATP synthase (Joliot & Joliot, 2008; Bailleul *et al.*, 2015). Accordingly, we also conclude that the $\Delta\psi_{\text{dark}}$ in *E. gracilis* indicates export of ATP from mitochondria into the chloroplast. In this respect, an ATP/ADP translocase isoform has been identified in the chloroplast proteome of *E. gracilis* (Novák Vančová *et al.*, 2020). Such ATP import may be useful during light exposure when ATP shortage occurs following the imbalance between the amount of ATP and NADPH produced by the activity of the photosynthetic electron transfer chain (Allen, 2002; Allen *et al.*, 2008; Bailleul *et al.*, 2015).

Previous studies (on diatoms, green algae and flowering plants) suggested that besides ATP, the energetic coupling between chloroplasts and mitochondria involves an exchange of reducing

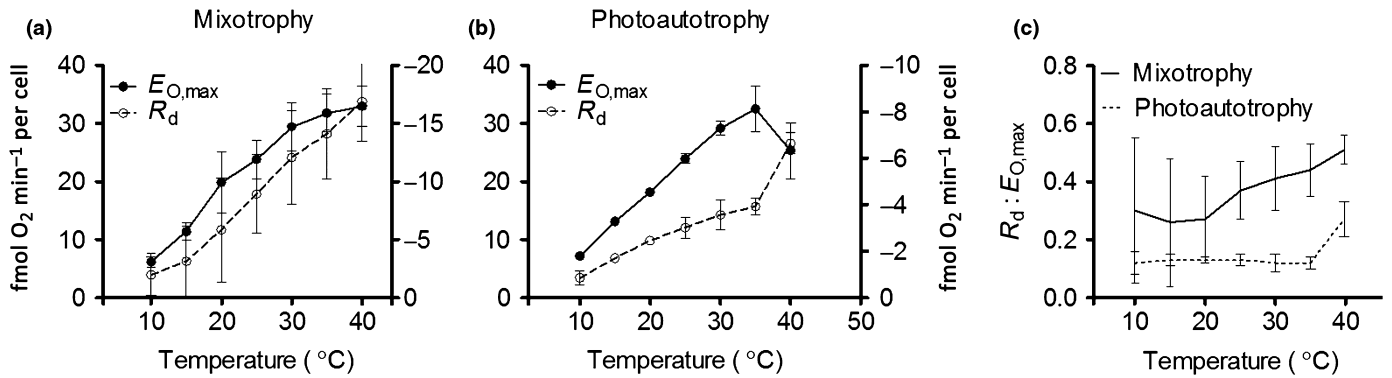


Fig. 2 Impact of change in temperature on gross maximal photosynthesis ($E_{O,max}$, left y-axis) and respiration (R_d , right y-axis) for *Euglena gracilis* cultivated in mixotrophic (a) and photoautotrophic (b) conditions. Measurements were conducted in the presence of 2 mM NaHCO_3 . (c) $R_d : E_{O,max}$ ratios as a function of increasing temperature. The connecting line fits through the raw data. All measurements were performed for at least three independent culture replicates. Vertical bars indicate the standard deviation.

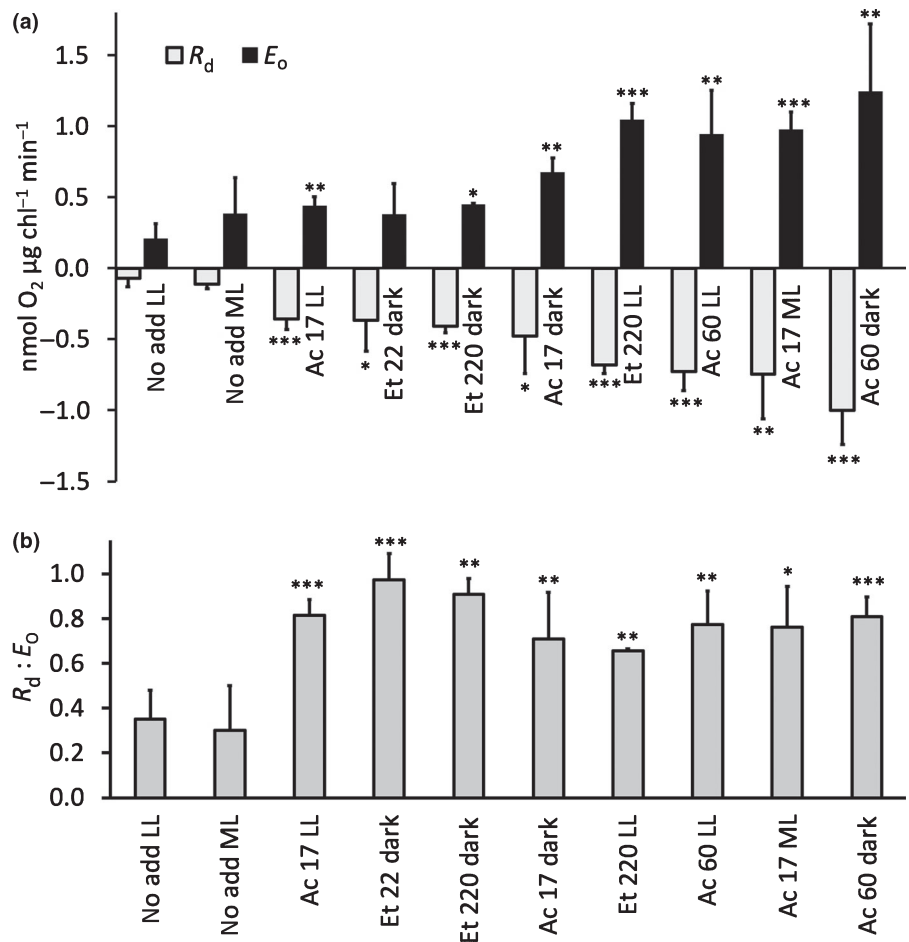


Fig. 3 Impact of addition of different organic carbon sources and/or variation in light intensity in culture on respiration (R_d), gross maximal photosynthesis ($E_{O,max}$) (a), and $R_d : E_{O,max}$ ratios (b) in *Euglena gracilis*. No add, no exogenous carbon source (TMP); Ac17, acetate 17 mM; Ac60, acetate 60 mM; Et22, ethanol 22 mM; Et220, ethanol 220 mM; LL, low light; ML, moderate light. No NaHCO_3 was added during the measurements. A total of 2×10^6 cells ml^{-1} were adjusted in the oximeter chamber. $E_{O,max}$ was measured during the last 3 min of 10 min illumination at $571 \mu\text{mol photons m}^{-2} \text{s}^{-1}$. Measurements were performed for at least two independent culture replicates. Vertical bars indicate the standard deviation. *, $P < 0.1$; **, $P < 0.05$; ***, $P < 0.01$; Student's t -test (values were compared with the E_O or R_d control values of the photoautotrophic condition (no add LL)).

equivalents by the malate-aspartate shuttle (Cardol *et al.*, 2003; Allen *et al.*, 2008; Noguchi & Yoshida, 2008; Bailleul *et al.*, 2015). This shuttle system comprises two soluble enzymes in each compartment, a malate dehydrogenase and an aspartate aminotransferase. In *E. gracilis*, isoforms of malate dehydrogenase have been identified in the chloroplast and mitochondrial proteomes (Hammond *et al.*, 2020; Novák Vanclová *et al.*, 2020) and aspartate aminotransferase activity has been identified in both the

mitochondrial and chloroplatic fractions (Collins *et al.*, 1975). AOAA, an inhibitor of the aspartate aminotransferase (Cornell *et al.*, 1984), had an inhibitory effect of *c.* 40% and 70% on R_d and E_O , respectively, in mixotrophy (Fig. 4b,c) (t -test; R_d , $P = 0.04$; $E_{O,max}$, $P = 0.0001$). This indicated that exchange of reducing equivalents by malate-aspartate shuttle between cell compartments is critical in the interaction between photosynthesis and respiration in mixotrophic conditions. By contrast, in the

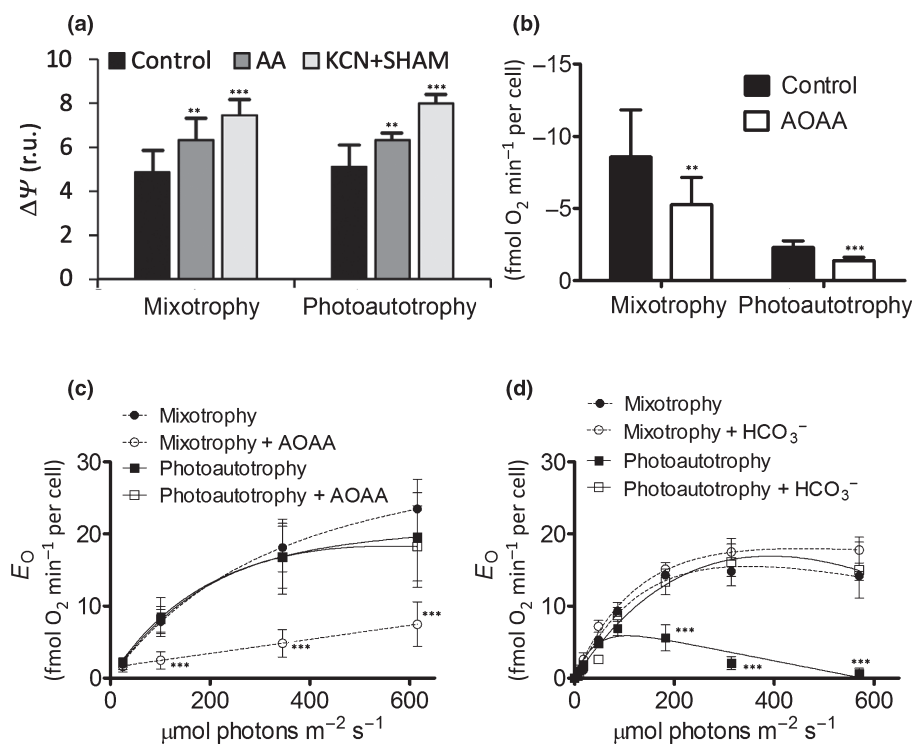


Fig. 4 (a) Impact of mitochondrial respiration inhibition (by potassium cyanide (KCN) and salicylhydroxamic acid (SHAM)), on the *Euglena gracilis* development of trans-thylakoid electric field ($\Delta\Psi$) induced by a series of single turnover flashes. r.u., units relative to one charge separation of both photosystem I (PSI) and PSII monitored by electrochromic shift at 510 nm (Supporting Information Fig. S1). (b, c) Impact of aspartate aminotransferase inhibition by aminooxyacetic acid (AOAA) on dark respiration (R_d) and gross oxygen exchange rate (E_O) of *E. gracilis* cultivated in mixotrophic and photoautotrophic conditions. A total of 5×10^5 cells ml^{-1} were adjusted in the oximeter chamber. Each light step (photosynthetic photon flux density (PPFD) of 25, 100, 345 and 615 $\mu\text{mol photons m}^{-2} \text{s}^{-1}$) was held for 2 min. (d) *Euglena gracilis* E_O with and without addition of NaHCO_3 (10 mM) in mixotrophic and photoautotrophic conditions. A total of 2×10^6 cells ml^{-1} were adjusted in the oximeter chamber. Each light step (PPFD of 7, 18, 48, 86, 182, 314 and 570 $\mu\text{mol photons m}^{-2} \text{s}^{-1}$) was held for 5 min. All measurements were performed for at least three independent culture replicates. Vertical bars indicate the standard deviation. *, $P < 0.1$; **, $P < 0.05$; ***, $P < 0.01$; Student's *t*-test (values were compared with the values of control cells).

photoautotrophic condition, the absence of an effect of AOAA on photosynthesis (Fig. 4c) (*t*-test; $E_{O,\text{max}}$, $P = 0.73$) despite a 40% decrease of R_d (Fig. 4b) (*t*-test, $P = 0.003$) may indicate that exchange of reducing equivalents could occur through a different pathway (e.g. glycerol-3-phosphate shuttle (Shen *et al.*, 2003) or the glycolate/glycerate transporter involved in photorespiration (Dellero *et al.*, 2016)). Alternatively, this result suggests that in the photoautotrophic condition, ATP import or CO_2 availability in the chloroplast is limiting for photosynthesis, rather than the capacity to export reducing equivalents out of the chloroplast. To test this latter hypothesis, we assessed the photosynthetic activity in the presence and absence of extemporaneous NaHCO_3 addition (using a higher cell concentration in the oximeter chamber) during consecutive long steps of increasing light intensity. CO_2 limitation in the photoautotrophic condition was indicated by the progressive decrease of E_O in the absence of NaHCO_3 (from 16 to 2 $\text{fmol O}_2 \text{ min}^{-1}$ per cell at saturating light intensity) (two-way ANOVA, $P < 0.0001$), a decline that did not occur in mixotrophy (Fig. 4d).

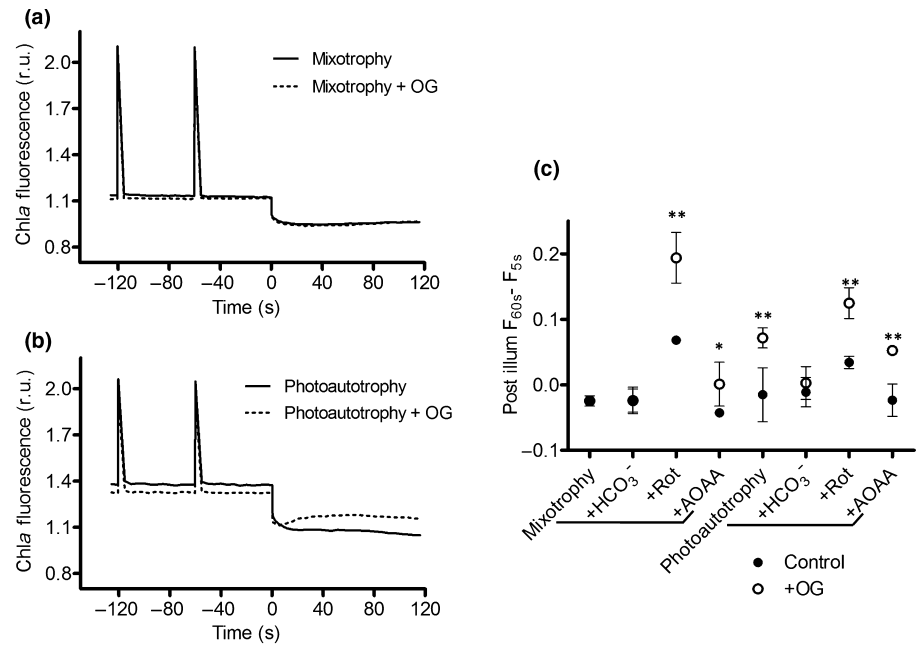
In a next step, we probed the redox poise in the stroma in the light. In green plants, the accumulation of reducing power (i.e. reduced ferredoxin (Fd) or NADPH) in the stroma occurs notably under high light regime. As a consequence, post-illumination NADPH (or Fd) plastoquinone oxidoreductase activity leads to

nonphotochemical reduction of the plastoquinone pool in the dark. Therefore, the accumulation of reducing power can be evidenced as changes in the post-illumination fluorescence (Gotoh *et al.*, 2010). The use of an inhibitor of the plastoquinol terminal oxidase (PTOX), octyl gallate (Josse *et al.*, 2003), further reveals the extent of nonphotochemical reduction of the plastoquinone pool. In *E. gracilis*, in mixotrophic conditions, post-illumination Chl fluorescence increase was observed only in the presence of rotenone or AOAA (Fig. 5a,c). This indicates that reducing power is accumulated in the stroma when the mitochondrial respiration or the malate shuttle were inhibited. In photoautotrophic conditions, post-illumination increase in Chl fluorescence was observed even in the absence of rotenone or AOAA and was abolished in the presence of bicarbonate (Fig. 5b,c). These results reinforce the idea that the limiting step of photosynthetic electron transport is CO_2 availability in photoautotrophy, while balancing ATP/NADPH ratio is critical in mixotrophy.

Different mechanisms of chloroplast–mitochondrion energetic coupling in mixotrophy and photoautotrophy

We investigated the main responses of central carbon metabolism and electron transfer pathways in *E. gracilis* grown

Fig. 5 Influence of mitochondrial inhibitors and bicarbonate addition on the stromal reducing power in *Euglena gracilis*. Chlorophyll fluorescence of *E. gracilis* cells grown in mixotrophy (a) or photoautotrophy (b) was monitored during the post-illumination period in the absence (control) or presence of octyl gallate (OG; 10 μ M). Time axis indicates the dark phase after 12 min of illumination. Chlorophyll fluorescence changes in the post-illumination phase were evaluated by the difference between fluorescence values at second 60 and 5 of this phase (c) in either the presence or absence of OG in addition to sodium bicarbonate (NaHCO_3 ; 10 mM), rotenone (Rot; 100 μ M) or aminooxyacetic acid (AOAA; 5 mM). All measurements were performed for at least two independent culture replicates. Vertical bars indicate standard deviation. *, $P < 0.1$; **, $P < 0.05$; Student's t -test (values were compared with the values of cells without OG addition).



in mixotrophy or in photoautotrophy. iTRAQ-based comparative proteomics identified a total of 544 proteins, including several enzymes involved in the central carbon metabolism pathways (Krebs cycle, Calvin cycle, glycolysis, beta-oxidation of fatty acid, lipid synthesis, respiratory and photosynthetic electron transfer chains, etc.) (Table S1). Among them, 112 proteins showed a significant \log_2 -fold increase or decrease (in the ratio of normalized protein abundance) depending on the trophic state (Table S2). In the mixotrophic condition, among the 53 proteins involved in carbon metabolism and electron transfer, mitochondrial proteins were more abundant, while chloroplastic and cytoplasmic proteins (Calvin cycle, glycolysis, and AA biosynthesis pathways) were relatively less abundant (Fig. 6). This mirrors the higher $R_d : E_{O,max}$ ratio (Figs 1b, 3c). The TEM micrographs of *E. gracilis* (Figs 8, S7) also revealed a higher number of mitochondrial sections per cell in mixotrophy and larger individual chloroplastic section area in photoautotrophy (Table 1). This translated into a lower ratio (*c.* 60%) between total area of chloroplastic sections per cell relative to mitochondrial sections in mixotrophy (one-way ANOVA, $P < 0.01$) (Table 1). The absence of difference in the Chl content per cell suggests that the stroma is relatively larger in photoautotrophy. Among mitochondrial proteins, the ATP-dependent acetyl-CoA synthase (ACS, which converts acetate to acetyl-CoA) and bifunctional isocitrate lyase/malate synthase (ICL-MAS, which cleaves isocitrate into succinate and glyoxylate, and further synthesizes malate from glyoxylate and acetyl-CoA) were found to be more abundant in mixotrophy. This increase of ACS and ICL-MAS reflects a shift in the metabolism to assimilate acetate into 4C compounds by bypassing the two decarboxylating steps of the Krebs cycle. Several components of the respiratory chain CI, CII (succinate dehydrogenase), CIII, CIV and CV (F_1F_0 ATP synthase), along with the ADP/ATP translocase and the inorganic phosphate carrier, were also more

abundant in mixotrophy. This increase of ATP synthesis capacity by oxidative phosphorylation is in agreement with the higher respiratory rates in mixotrophy than in photoautotrophy (Figs 1a, 2, 4b), and may fuel anabolic reactions inside the mitochondria (e.g. for acetate assimilation), in the cytosol (e.g. neoglucogenesis) and/or in the chloroplast (e.g. for CO_2 assimilation). In *Chlorella sorokiniana*, mixotrophy was not associated with an increase in the transcript abundance of ICL and respiratory-chain components, but with an upregulation of glycolate oxidase and serine hydroxymethyltransferase (SHMT), two enzymes involved in photorespiration (Cecchin *et al.*, 2018). By contrast, mixotrophy in *E. gracilis* caused a decline in glycine cleavage system (P and H proteins) and SHMT. In *E. gracilis*, these proteins are present in the mitochondrial fractions (Hammond *et al.*, 2020) and participate in photorespiration by catalysing oxidative decarboxylation of glycine into serine. Only two photosynthetic electron transfer chain components (PSII H subunit and beta subunit of F_1F_0 ATP synthase) were more abundant in mixotrophy (Fig. 6). These changes were not, however, accompanied by a difference in the $E_{O,max}$ between cells in mixotrophy and photoautotrophy (Figs 2, 4c,d) (provided that NaHCO_3 is added to the photoautotrophic cells during the measurement to limit RuBisCO oxygenase activity). On average, there is twice the number of pyrenoids (relative to the chloroplastic sections) in photoautotrophy than in mixotrophy or photoautotrophy + 5% CO_2 (Table 1). Although not statistically significant, this difference is supported by higher amounts of RuBisCO large subunit, Rubisco activase and RuBisCO large subunit-binding protein subunit beta specifically in photoautotrophy (Table S1). Altogether, this indicates that *E. gracilis* cells in photoautotrophy are more prone to photorespiration than when cells rely on an exogenous reduced carbon source (here acetate). Decarboxylating enzymes (isocitrate dehydrogenase and malic enzyme) are

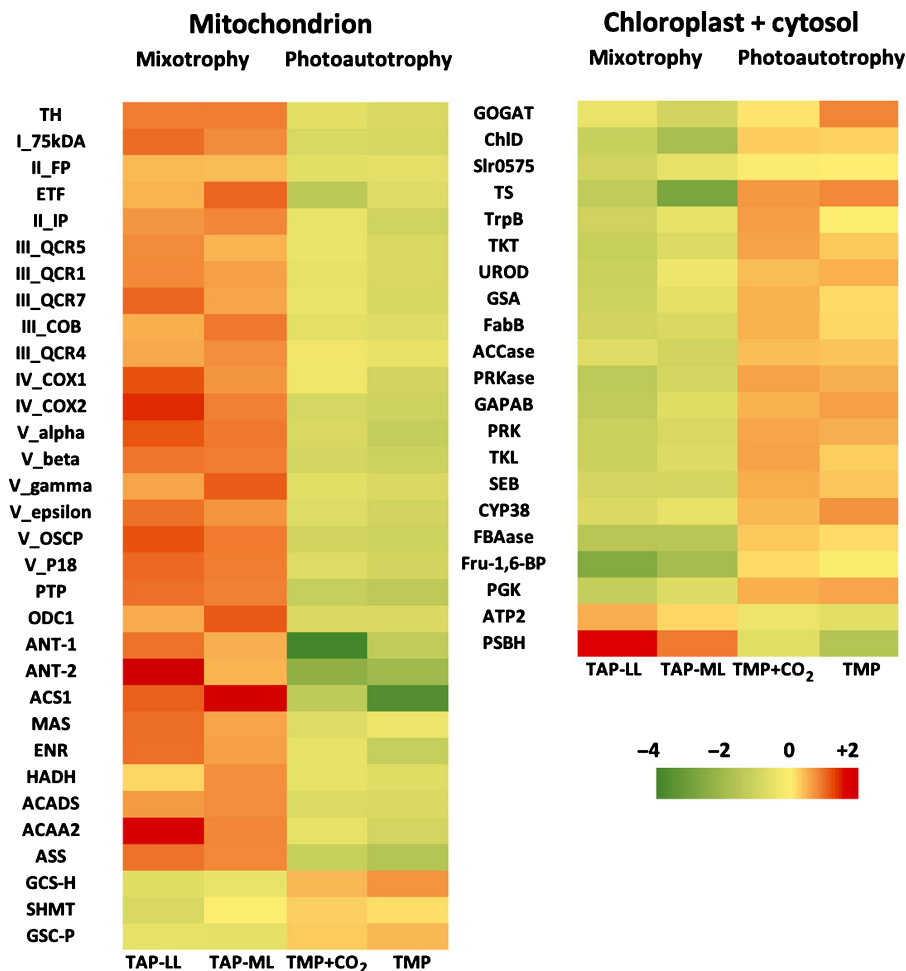


Fig. 6 Heat map generated from iTRAQ LC-MS quantitative proteomics analysis of *Euglena gracilis* cells in mixotrophic or photoautotrophic conditions. Only proteins participating in primary carbon metabolism and showing significant differences (log₂-fold change) in relative abundance between mixotrophic and photoautotrophic conditions are presented. Full datasets can be found in Supporting Information Tables S1, S2. Samples are arranged in columns, proteins in rows. Red shades, increased abundance; green shades, reduced abundance; yellow, median expression.

also more abundant specifically in TMP (Table S1). This may reflect the cellular need for CO₂ uptake and CO₂-concentrating mechanism activity (Giordano *et al.*, 2005). During photorespiration, RuBisCO oxygenase activity generates phosphoglycolate in addition to phosphoglycerate. Phosphoglycolate is converted to glycolate which can be imported into the mitochondrion in *E. gracilis* (Collins *et al.*, 1975). Glycolate dehydrogenase and glyoxylate-glutamate aminotransferase, two other photorespiratory enzymes which are usually localized in the peroxisome in other species, are also localized in the mitochondrion in *E. gracilis* and convert glycolate into glycine (Collins *et al.*, 1975; Horrum & Schwartzbach, 1980; Hammond *et al.*, 2020). Interestingly, glyoxylate-glutamate aminotransferase is not inhibited by AOAA (Horváth & Wanders, 1995). The lack of effect of AOAA addition on E_O specifically in photoautotrophy (Fig. 4c) is therefore in line with an active photorespiration, rather than an export of reducing equivalents through the malate shuttle that occurs in mixotrophy. Together with NADH produced by oxidation of glycine by glycine cleavage system and SHMT, glycolate oxidation may contribute directly to fuel mitochondrial electron transfer chain and ATP synthesis. This suggestion is in line with the observation that glycolate-dependent O₂ uptake by *E. gracilis* mitochondria is inhibited by AA or cyanide (Collins *et al.*, 1975). The negative impact of R_d

inhibition on E_O in photoautotrophic condition (Fig. 1a) could thus be caused by the loss of mitochondrial capacity to reoxidize NAD(P)H produced by photorespiratory enzymes inside the mitochondria. Concomitantly, the expected slowing down of the decarboxylative enzymes of the Krebs cycle and of photorespiration should limit the amount of CO₂ available for RuBisCO. A metabolic scheme summarizing how mitochondrial respiratory activity interacts with photosynthesis in mixotrophy and photoautotrophy in *E. gracilis* is presented in Fig. 7.

Membrane contact sites between chloroplasts and mitochondria

In diatoms, it has been suggested that the chloroplast–mitochondrion energetic coupling could be favoured by an intracellular placing of the mitochondrial network in close proximity to the single chloroplast (Prihoda *et al.*, 2012; Flori *et al.*, 2017). It was recently shown that the extent of chloroplast–mitochondrion physical interaction varies greatly among phytoplanktonic species of different lineages, being high in the diatom *P. tricornutum* and low in *Symbiodinium* sp. or *Nannochloropsis* sp. (Uwizeye *et al.*, 2021). In *E. gracilis*, TEM micrographs (Figs 8, S7) also showed that c. 60–80% of mitochondrial sections localize close to chloroplasts, often at margins of chloroplast sections,

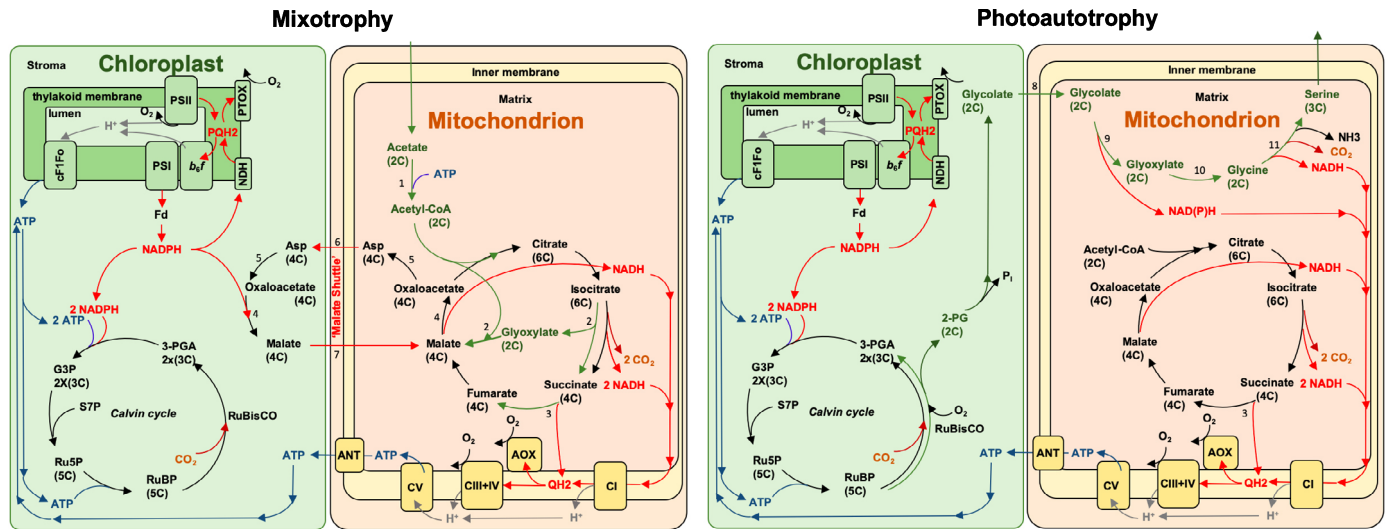


Fig. 7 Model of mitochondrial participation to photosynthesis regulation in mixotrophy and autotrophy in *Euglena gracilis*. Metabolic pathways reported in green are pathways with significant differences (\log_2 -fold change) in relative abundance between mixotrophic and photoautotrophic conditions (Fig. 5; Supporting Information Table S1). Red, blue, brown and grey arrows depict production/consumption of reducing equivalents (NAD(P)H, Quinone), ATP, carbon dioxide, and H^+ , respectively. Only pathways mentioned in the text are depicted. ANT, adenine nucleotide translocator or ADP/ATP translocase; AOX, alternative oxidase; Asp, aspartate; G3P, glyceraldehyde 3-phosphate; Fd, ferredoxin; 2-PG, 2-phosphoglycerate; 3-PGA, 3-phosphoglycerate; NDH, putative NADPH plastoquinone reductase; PQH₂, plastoquinol; PTOX, plastidial alternative oxidase; QH₂, ubiquinol; Ru5P, ribulose-5-phosphate; RuBP, ribulose-1,5-bisphosphate; S7P, sedoheptulose 7-phosphate; 1, acetyl-CoA synthetase; 2, bifunctional isocitrate dehydrogenase / malate synthase; 3, succinate dehydrogenase (respiratory-chain complex II); 4, NAD(P)H-dependant malate dehydrogenase; 5, aspartate transaminase; 6, glutamate/aspartate transporter; 7 malate/oxoglutarate transporter; 8, glycolate/glycerate transporter; 9, glycolate dehydrogenase; 10, glutamate : glyoxylate aminotransferase; 11, glycine cleavage system + serine hydroxymethyltransferase.

with no difference among the mixotrophic, photoautotrophic and photoautotrophic + 5% CO₂ conditions (Table 1) (one-way ANOVA, $P=0.18$). This confirmed previous observations that mitochondrial sections of *E. gracilis* tend to localize adjacent to the chloroplast in light-adapted cells (Wolken, 1967), but at the cell periphery in dark-adapted cells (Wolken, 1967; Pellegrini, 1980), which might relate to local concentration of oxygen (Wolken, 1967). The average distance between external membranes of chloroplasts and mitochondria was < 20–30 nm over 0.5 μm membrane segments (with no significant difference among conditions; one-way ANOVA, $P=0.22$), and no outer membrane fusion between organelles was observed (Figs 8, S7). Such membrane contact sites (MCSs) have been described to create microdomains that favour exchange of molecules between endoplasmic reticulum and different organelles in the photosynthetic cell (Pérez-Sancho *et al.*, 2016). Thus, we suggest that ATP, ADP and reducing equivalents, along with other molecules (including, e.g., glycolate, glycerate, HCO_3^-), underlying the energetic coupling between respiration and photosynthesis, might be efficiently transported across MCSs between chloroplasts and mitochondria in *E. gracilis*. Protein tethering complexes are required for the establishment of MCSs between endoplasmic reticulum and different organelles (Helle *et al.*, 2013) but it is not known if chloroplast–mitochondrion MCSs also depend on such complexes in photosynthetic organisms. Because *E. gracilis* chloroplasts are surrounded by three membranes, rather than two as in green plants or four as in diatoms, it will be of interest to elucidate the configuration of the MCSs and the diversity of transporters.

Conclusions

Following the evolutionary course of *E. gracilis*, which consisted of the acquisition of photosynthesis by a heterotrophic ancestor (euglenozoan) from a eukaryotic donor (green alga), the activities of mitochondria and chloroplasts are intimately coupled. This ensures the cell has an export of reducing equivalents from the chloroplasts towards mitochondria and an import of ATP into the chloroplasts to sustain photosynthetic CO₂ fixation. Under the mixotrophic condition, the energetic coupling of *E. gracilis* is very similar to what is proposed to occur in diatoms, for which the main driver of this interaction is thought to be the adjustment of the ATP/NADPH ratio in the chloroplast (Bailleul *et al.*, 2015). By contrast, other photosynthetic organisms (and especially those bearing green plastids), may rely primarily on AEPs located in the chloroplasts for controlling the cellular ATP/NADPH budget (Scheibe, 2004; Roberty *et al.*, 2014; Raven *et al.*, 2020). In the green alga *C. reinhardtii*, mitochondrial cooperation supplies extra ATP for photosynthesis when the chloroplast capacity of AEPs to supply ATP for CO₂ assimilation is compromised (Dang *et al.*, 2014). Information on AEPs in *E. gracilis* in the literature is, however, still scarce (e.g. Shimakawa *et al.*, 2017). The linear relationship between PSII relative electron transport rate and PSI + PSII photochemical rate, their insensitivity to AA (Fig. S8a,b), and the very low photochemical rate ($2.5 \pm 1.4 \text{ s}^{-1}$) in the presence of DCMU suggest, however, that the cyclic electron flow around PSI is not prominent in *E. gracilis*. Similarly, the linear relationship between PSII relative electron transport rate and E_{O} (Fig. S8c) suggests that cyclic electron flow

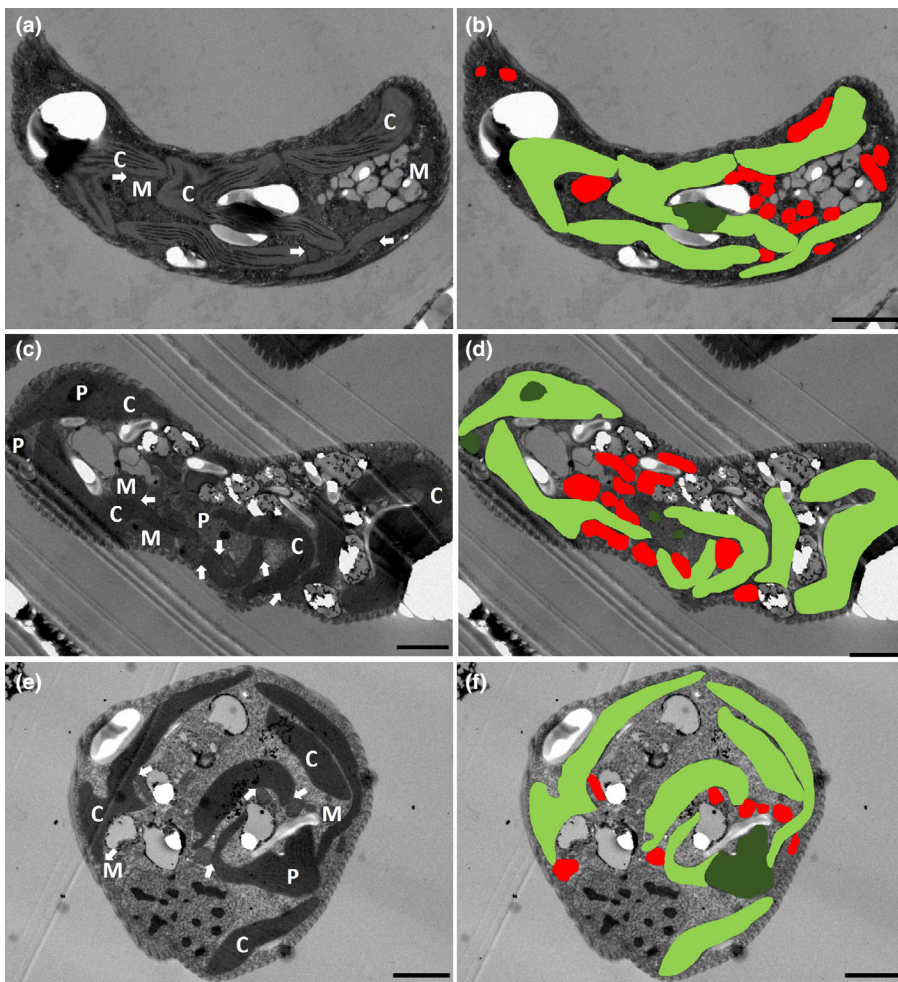


Fig. 8 Transmission electron micrographs illustrating subcellular organization of *Euglena gracilis* cultured in mixotrophy (a, b), photoautotrophy (c, d) and photoautotrophy + 5% CO₂ (e, f). Bars, 2 μm. (a, c, e) Arrows show the mitochondrial-chloroplasmic contacts; C, chloroplast; M, mitochondrion; P, pyrenoid. (b, d, f) Cell compartments are highlighted in colour (chloroplasts in light green, pyrenoids in dark green and mitochondria in red).

around PSII does not occur. Overall, these findings reinforce the idea that the energetic coupling between chloroplasts and mitochondria is crucial in *E. gracilis*. The mechanisms whereby the energetic coupling between photosynthesis and respiration occurs vary in relation to the trophic state of the cell (mixotrophic vs photoautotrophic). Under the photoautotrophic condition, the ATP demand for photorespiration and the CO₂-concentrating mechanism takes precedence over the chloroplastic NADPH excess. In *E. gracilis*, as in diatoms, the evolutionary and physiological advantages and/or disadvantages of relying mainly on the chloroplast to mitochondrion coupling are not clear. Such strong chloroplast–mitochondrion interdependence could make these organisms sensitive to any impairment of the respiratory activity, which would cause negative consequences on the photosynthetic apparatus as well. Cell ability to ensure that photosynthesis–respiration coupling is maintained through plastic metabolic responses (as we have shown for mixotrophic vs photoautotrophic conditions in *E. gracilis*) is therefore key to guarantee cell functioning. In addition, the presence of AEP in the chloroplast could help cells to compensate for possible respiratory impairments. Further studies are required to establish the role of AEPs (if any) in the regulation of the cellular ATP/NADPH budget (e.g. during conditions impairing respiration) in species such

as *E. gracilis* or *P. tricornutum* (diatom), characterized by having photosynthesis–respiration coupling as a major regulator of photosynthesis.

Acknowledgements




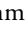

We thank Benjamin Bailleul (IBPC, Paris, France) for helpful discussions during the preparation of the manuscript. We thank Martin Charlier for technical help with growth experiments and Patricia Piscicelli for technical help with TEM. We thank Nataly Hidalgo for her statistical advice. PC acknowledges financial support from the Belgian Fonds de la Recherche Scientifique FRS-FNRS (PDR T.0032) and European Research Council (ERC, H2020-EU BEAL project 682580). PC is Senior Research Associate from FNRS.

Author contributions

GG, FVdL, DB, MP and PC conceived the research. PM, HD, EP and JC carried out the proteomics analysis. MT performed the TEM analysis. GG, FVdL, EP, MP and PC performed the physiological analyses and analysed data. MP and PC wrote the manuscript. MP and PC share senior authorship. GG and FVdL

contributed equally to this work. All authors read and approved the manuscript.

ORCID

Denis Baurain  <https://orcid.org/0000-0003-2388-6185>
 Pierre Cardol  <https://orcid.org/0000-0001-9799-0546>
 Gwenaëlle Gain  <https://orcid.org/0000-0002-3871-3300>
 Pierre Morsomme  <https://orcid.org/0000-0001-7780-7230>
 Mattia Pierangelini  <https://orcid.org/0000-0002-6166-8472>

Data availability

The data that support the findings of this study are available from the corresponding authors upon reasonable request. The data that supports the proteomics are available in the supplementary material.

References

- Allen AE, LaRoche J, Maheswari U, Lommer M, Schauer N, Lopez PJ, Finazzi G, Fernie AR, Bowler C. 2008. Whole-cell response of the pennate diatom *Phaeodactylum tricorutum* to iron starvation. *Proceedings of the National Academy of Sciences, USA* 105: 10438–10443.
- Allen JF. 2002. Photosynthesis of ATP-electrons, proton pumps, rotors, and poise. *Cell* 110: 273–276.
- Atkin OK, Tjoelker MG. 2003. Thermal acclimation and the dynamic response of plant respiration to temperature. *Trends in Plant Science* 8: 343–351.
- Bailleul B, Berne N, Murik O, Petroutsos D, Prihoda J, Tanaka A, Villanova V, Bligny R, Flori S, Falconet D *et al.* 2015. Energetic coupling between plastids and mitochondria drives CO₂ assimilation in diatoms. *Nature* 524: 366–369.
- Bailleul B, Cardol P, Breyton C, Finazzi G. 2010. Electrochromism: a useful probe to study algal photosynthesis. *Photosynthesis Research* 106: 179–189.
- Bennett MS, Wiegert KE, Triemer RE. 2012. Comparative chloroplast genomics between *Euglena viridis* and *Euglena gracilis* (Euglenophyta). *Phycologia* 51: 711–718.
- Berry J, Bjorkman O. 1980. Photosynthetic response and adaptation to temperature in higher plants. *Annual Review of Plant Physiology* 31: 491–543.
- Bradford MM. 1976. A rapid and sensitive method for the quantitation of microgram quantities of protein utilizing the principle of protein-dye binding. *Analytical Biochemistry* 72: 248–254.
- Cardol P, Alric J, Girard-Bascou J, Franck F, Wollman FA, Finazzi G. 2009. Impaired respiration discloses the physiological significance of state transitions in *Chlamydomonas*. *Proceedings of the National Academy of Sciences, USA* 106: 15979–15984.
- Cardol P, Forti G, Finazzi G. 2011. Regulation of electron transport in microalgae. *Biochimica et Biophysica Acta (BBA)–Bioenergetics* 1807: 912–918.
- Cardol P, Gloire G, Havaux M, Remacle C, Matagne R, Franck F. 2003. Photosynthesis and state transitions in mitochondrial mutants of *Chlamydomonas reinhardtii* affected in respiration. *Plant Physiology* 133: 2010–2020.
- Castro-Guerrero NA, Krab K, Moreno-Sánchez R. 2004. The alternative respiratory pathway of *Euglena* mitochondria. *Journal of Bioenergetics and Biomembranes* 36: 459–469.
- Cecchin M, Benfatto S, Griggio F, Mori A, Cazzaniga S, Vitulo N, Delledonne M, Ballottari M. 2018. Molecular basis of autotrophic vs mixotrophic growth in *Chlorella sorokiniana*. *Scientific Reports* 8: 1–13.
- Chapman SP, Paget CM, Johnson GN, Schwartz JM. 2015. Flux balance analysis reveals acetate metabolism modulates cyclic electron flow and alternative glycolytic pathways in *Chlamydomonas reinhardtii*. *Frontiers in Plant Science* 6: 474.
- Collins N, Brown RH, Merrett MJ. 1975. Oxidative phosphorylation during glycolate metabolism in mitochondria from phototrophic *Euglena gracilis*. *Biochemical Journal* 150: 373–377.
- Cornell NW, Zuurendonk PF, Kerich MJ, Straight CB. 1984. Selective inhibition of alanine aminotransferase and aspartate aminotransferase in rat hepatocytes. *Biochemical Journal* 220: 707–716.
- Dang KV, Plet J, Tolleter D, Jokel M, Cuiné S, Carrier P, Auroy P, Richaud P, Johnson X, Alric J *et al.* 2014. Combined increases in mitochondrial cooperation and oxygen photoreduction compensate for deficiency in cyclic electron flow in *Chlamydomonas reinhardtii*. *Plant Cell* 26: 3036–3050.
- Dellero Y, Jossier M, Schmitz J, Maurino VG, Hodges M. 2016. Photorespiratory glycolate–glyoxylate metabolism. *Journal of Experimental Botany* 67: 3041–3052.
- Falkowski PG, Dubinsky Z, Wyman K. 1985. Growth-irradiance relationships in phytoplankton. *Limnology and Oceanography* 30: 311–321.
- Feikema WO, Marosvölgyi MA, Lavaud J, Van Gorkom HJ. 2006. Cyclic electron transfer in photosystem II in the marine diatom *Phaeodactylum tricorutum*. *Biochimica et Biophysica Acta (BBA)–Bioenergetics* 1757: 829–834.
- Flori S, Jouneau PH, Bailleul B, Gallet B, Estrozi LF, Moriscot C, Bastien O, Eicke S, Schober A, Bártulos CR *et al.* 2017. Plastid thylakoid architecture optimizes photosynthesis in diatoms. *Nature Communications* 8: 1–9.
- Geider RJ, Osborne BA. 1989. Respiration and microalgal growth: a review of the quantitative relationship between dark respiration and growth. *New Phytologist* 112: 327–341.
- Giordano M, Beardall J, Raven JA. 2005. CO₂ concentrating mechanisms in algae: mechanisms, environmental modulation, and evolution. *Annual Review of Plant Biology* 56: 99–131.
- Gotoh E, Matsumoto M, Ogawa KI, Kobayashi Y, Tsuyama M. 2010. A qualitative analysis of the regulation of cyclic electron flow around photosystem I from the post-illumination chlorophyll fluorescence transient in *Arabidopsis*: a new platform for the in vivo investigation of the chloroplast redox state. *Photosynthesis Research* 103: 111–123.
- Hammond MJ, Nenarokova A, Butenko A, Zoltner M, Dobáková EL, Field MC, Lukeš J. 2020. A uniquely complex mitochondrial proteome from *Euglena gracilis*. *Molecular Biology and Evolution* 37: 2173–2191.
- Helle SC, Kanfer G, Kolar K, Lang A, Michel AH, Kornmann B. 2013. Organization and function of membrane contact sites. *Biochimica et Biophysica Acta (BBA)–Molecular Cell Research* 1833: 2526–2541.
- Horrum MA, Schwartzbach SD. 1980. Nutritional regulation of organelle biogenesis in *Euglena*: repression of chlorophyll and NADP-glyceraldehyde-3-phosphate dehydrogenase synthesis. *Plant Physiology* 65: 382–386.
- Horváth VAP, Wanders RJ. 1995. Aminooxy acetic acid: a selective inhibitor of alanine: glyoxylate aminotransferase and its use in the diagnosis of primary hyperoxaluria type I. *Clinica Chimica Acta* 243: 105–114.
- Iglesias-Prieto R, Matta JL, Robins WA, Trench RK. 1992. Photosynthetic response to elevated temperature in the symbiotic dinoflagellate *Symbiodinium microadriaticum* in culture. *Proceedings of the National Academy of Sciences, USA* 89: 10302–10305.
- Jackson C, Knoll AH, Chan CX, Verbruggen H. 2018. Plastid phylogenomics with broad taxon sampling further elucidates the distinct evolutionary origins and timing of secondary green plastids. *Scientific Reports* 8: 1–10.
- Joliot P, Joliot A. 2008. Quantification of the electrochemical proton gradient and activation of ATP synthase in leaves. *Biochimica et Biophysica Acta (BBA)–Bioenergetics* 1777: 676–683.
- Josse EM, Alcaraz JP, Labouré AM, Kuntz M. 2003. In vitro characterization of a plastid terminal oxidase (PTOX). *European Journal of Biochemistry* 270: 3787–3794.
- Kamalanathan M, Dao LHT, Chaisutyakorna P, Gleadow R, Beardall J. 2017. Photosynthetic physiology of *Scenedesmus* sp. (Chlorophyceae) under photoautotrophic and molasses-based heterotrophic and mixotrophic conditions. *Phycologia* 56: 666–674.
- Kammers K, Cole RN, Tiengwe C, Ruczinski I. 2015. Detecting significant changes in protein abundance. *EuPA Open Proteomics* 7: 11–19.
- Karsten U, Holzinger A. 2012. Light, temperature, and desiccation effects on photosynthetic activity, and drought-induced ultrastructural changes in the green alga *Klebsormidium dissectum* (Streptophyta) from a high alpine soil crust. *Microbial Ecology* 63: 51–63.
- Kaye Y, Huang W, Clowez S, Saroussi S, Idoine A, Sanz-Luque E, Grossman AR. 2019. The mitochondrial alternative oxidase from *Chlamydomonas*

- reinhardtii* enables survival in high light. *Journal of Biological Chemistry* 294: 1380–1395.
- Krnáčová K, Rýdlová I, Vinarčíková M, Krajčovič J, Vesteg M, Horváth A. 2015. Characterization of oxidative phosphorylation enzymes in *Euglena gracilis* and its white mutant strain *W_{gm}ZOJL*. *FEBS Letters* 589: 687–694.
- Larkum AW, Lockhart PJ, Howe CJ. 2007. Shopping for plastids. *Trends in Plant Science* 12: 189–195.
- McDonald AE, Ivanov AG, Bode R, Maxwell DP, Rodermeil SR, Hüner NP. 2011. Flexibility in photosynthetic electron transport: the physiological role of plastoquinol terminal oxidase (PTOX). *Biochimica et Biophysica Acta (BBA)–Bioenergetics* 1807: 954–967.
- Miranda-Astudillo HV, Yadav KNS, Colina-Tenorio L, Bouillenne F, Degand H, Morsomme P, Boekema EJ, Cardol P. 2018. The atypical subunit composition of respiratory complexes I and IV is associated with original extra structural domains in *Euglena gracilis*. *Scientific Reports* 8: 1–13.
- Murik O, Tirichine L, Prihoda J, Thomas Y, Araújo WL, Allen AE, Fernie AR, Bowler C. 2019. Downregulation of mitochondrial alternative oxidase affects chloroplast function, redox status and stress response in a marine diatom. *New Phytologist* 221: 1303–1316.
- Noguchi K, Yoshida K. 2008. Interaction between photosynthesis and respiration in illuminated leaves. *Mitochondrion* 8: 87–99.
- Novák Vanclová AM, Zoltner M, Kelly S, Soukal P, Záhonová K, Füssy Z, Ebenezer TE, Lacová Dobaková E, Eliáš M, Lukeš J *et al.* 2020. Metabolic quirks and the colourful history of the *Euglena gracilis* secondary plastid. *New Phytologist* 225: 1578–1592.
- Padfield D, Yvon-Durocher G, Buckling A, Jennings S, Yvon-Durocher G. 2016. Rapid evolution of metabolic traits explains thermal adaptation in phytoplankton. *Ecology Letters* 19: 133–142.
- Pellegrini M. 1980. Three-dimensional reconstruction of organelles in *Euglena gracilis* Z.I. Qualitative and quantitative changes of chloroplasts and mitochondrial reticulum in synchronous photoautotrophic culture. *Journal of Cell Science* 43: 137–166.
- Perez E, Lapaille M, Degand H, Cilibrasi L, Villavicencio-Queijeiro A, Morsomme P, González-Halphen D, Field MC, Remacle C, Baurain D *et al.* 2014. The mitochondrial respiratory chain of the secondary green alga *Euglena gracilis* shares many additional subunits with parasitic Trypanosomatidae. *Mitochondrion* 19: 338–349.
- Pérez-Sancho J, Tilsner J, Samuels AL, Botella MA, Bayer EM, Rosado A. 2016. Stitching organelles: organization and function of specialized membrane contact sites in plants. *Trends in Cell Biology* 26: 705–717.
- Pierangelini M, Glaser K, Mikhailyuk T, Karsten U, Holzinger A. 2019. Light and dehydration but not temperature drive photosynthetic adaptations of basal streptophytes (*Hormidiella*, *Streptosarcina* and *Streptoflum*) living in terrestrial habitats. *Microbial Ecology* 77: 380–393.
- Pierangelini M, Thiry M, Cardol P. 2020. Different levels of energetic coupling between photosynthesis and respiration do not determine the occurrence of adaptive responses of Symbiodiniaceae to global warming. *New Phytologist* 228: 855–868.
- Polukhina I, Fristedt R, Dinc E, Cardol P, Croce R. 2016. Carbon supply and photoacclimation cross talk in the green alga *Chlamydomonas reinhardtii*. *Plant Physiology* 172: 1494–1505.
- Powell DW, Weaver CM, Jennings JL, McAfee KJ, He Y, Weil PA, Link AJ. 2004. Cluster analysis of mass spectrometry data reveals a novel component of SAGA. *Molecular and Cellular Biology* 24: 7249–7259.
- Prelle LR, Graiff A, Gründling-Pfaff S, Sommer V, Kuriyama K, Karsten U. 2019. Photosynthesis and respiration of Baltic Sea benthic diatoms to changing environmental conditions and growth responses of selected species as affected by an adjacent peatland (Hütelmoor). *Frontiers in Microbiology* 10: 1500.
- Prihoda J, Tanaka A, de Paula WB, Allen JF, Tirichine L, Bowler C. 2012. Chloroplast-mitochondria cross-talk in diatoms. *Journal of Experimental Botany* 63: 1543–1557.
- Raghavendra AS, Padmasree K. 2003. Beneficial interactions of mitochondrial metabolism with photosynthetic carbon assimilation. *Trends in Plant Science* 8: 546–553.
- Raven JA, Beardall J. 2016. Dark respiration and organic carbon loss. In: Borowitzka M, Beardall J, Raven J, eds. *The physiology of microalgae. Developments in applied phycology*. Cham, Switzerland: Springer, 129–140.
- Raven JA, Beardall J, Quigg A. 2020. Light-driven oxygen consumption in the water-water cycles and photorespiration, and light stimulated mitochondrial respiration. In: Larkum A, Grossman A, Raven J, eds. *Photosynthesis in algae: biochemical and physiological mechanisms*. Cham, Switzerland: Springer, 161–178.
- Remacle C, Cardol P, Coosemans N, Gaisne M, Bonnefoy N. 2006. High-efficiency biolistic transformation of *Chlamydomonas* mitochondria can be used to insert mutations in complex I genes. *Proceedings of the National Academy of Sciences, USA* 103: 4771–4776.
- Ritchie ME, Phipson B, Wu DI, Hu Y, Law CW, Shi W, Smyth GK. 2015. limma powers differential expression analyses for RNA-sequencing and microarray studies. *Nucleic Acids Research* 43: e47.
- Ritchie RJ. 2006. Consistent sets of spectrophotometric chlorophyll equations for acetone, methanol and ethanol solvents. *Photosynthesis Research* 89: 27–41.
- Roberty S, Bailleul B, Berne N, Franck F, Cardol P. 2014. PSI Mehler reaction is the main alternative photosynthetic electron pathway in *Symbiodinium* sp., symbiotic dinoflagellates of cnidarians. *New Phytologist* 204: 81–91.
- Schaum CE, Barton S, Bestion E, Buckling A, Garcia-Carreras B, Lopez P, Lowe L, Pawar S, Smirnoff N, Trimmer M *et al.* 2017. Adaptation of phytoplankton to a decade of experimental warming linked to increased photosynthesis. *Nature Ecology & Evolution* 1: 1–7.
- Scheibe R. 2004. Malate valves to balance cellular energy supply. *Physiologia Plantarum* 120: 21–26.
- Shen W, Wei Y, Dauk M, Zheng Z, Zou J. 2003. Identification of a mitochondrial glycerol-3-phosphate dehydrogenase from *Arabidopsis thaliana*: evidence for a mitochondrial glycerol-3-phosphate shuttle in plants. *FEBS Letters* 536: 92–96.
- Shimakawa G, Matsuda Y, Nakajima K, Tamoi M, Shigeoka S, Miyake C. 2017. Diverse strategies of O₂ usage for preventing photo-oxidative damage under CO₂ limitation during algal photosynthesis. *Scientific Reports* 7: 1–9.
- Szopinska A, Degand H, Hochstenbach JF, Nader J, Morsomme P. 2011. Rapid response of the yeast plasma membrane proteome to salt stress. *Molecular & Cellular Proteomics* 10: M111-009589.
- Treves H, Raanan H, Kedem I, Murik O, Keren N, Zer H, Berkowicz SM, Giordano M, Norici A, Shotland Y *et al.* 2016. The mechanisms whereby the green alga *Chlorella obadii*, isolated from desert soil crust, exhibits unparalleled photodamage resistance. *New Phytologist* 210: 1229–1243.
- Turmel M, Gagnon MC, O'Kelly CJ, Otis C, Lemieux C. 2009. The chloroplast genomes of the green algae *Pyramimonas*, *Monomastix*, and *Pycnococcus* shed new light on the evolutionary history of prasinophytes and the origin of the secondary chloroplasts of euglenids. *Molecular Biology and Evolution* 26: 631–648.
- Uwizeye C, Decelle J, Jouneau P, Flori S, Gallet B, Keck JB, Dal Bo D, Moriscot C, Seydoux C, Chevalier F *et al.* 2021. Morphological bases of phytoplankton energy management and physiological responses unveiled by 3D subcellular imaging. *Nature Communications* 12: 1–12.
- Vaudel M, Burkhart JM, Zahedi RP, Oveland E, Berven FS, Sickmann A, Martens L, Barsnes H. 2015. PeptideShaker enables reanalysis of MS-derived proteomics data sets. *Nature Biotechnology* 33: 22–24.
- Wessel DM, Flüggé UI. 1984. A method for the quantitative recovery of protein in dilute solution in the presence of detergents and lipids. *Analytical Biochemistry* 138: 141–143.
- Wilken S, Schuurmans JM, Matthijs HC. 2014. Do mixotrophs grow as photoheterotrophs? Photophysiological acclimation of the chrysophyte *Ochromonas danica* after feeding. *New Phytologist* 204: 882–889.
- Wolken JJ. 1967. *Euglena: an experimental organism for biochemical and biophysical studies*, 2nd edn. New York, NY, USA: Appleton-Century-Crofts.
- Yadav KS, Miranda-Astudillo HV, Colina-Tenorio L, Bouillenne F, Degand H, Morsomme P, González-Halphen D, Boekema EJ, Cardol P. 2017. Atypical composition and structure of the mitochondrial dimeric ATP synthase from *Euglena gracilis*. *Biochimica et Biophysica Acta (BBA)–Bioenergetics* 1858: 267–275.

Supporting Information

Additional Supporting Information may be found online in the Supporting Information section at the end of the article.

Fig. S1 Electrochromic shift spectrum and linearity in *Euglena gracilis* cultivated mixotrophically and photoautotrophically.

Fig. S2 Impact of inhibitors on Chl fluorescence in *Euglena gracilis* cultured in mixotrophy and in photoautotrophy.

Fig. S3 NPQ in *Euglena gracilis* cells grown in mixotrophy or in photoautotrophy.

Fig. S4 Impact of octyl gallate (OG) and salicylhydroxamic acid (SHAM) on dark respiration (R_d) in *Euglena gracilis* cultivated in mixotrophic and photoautotrophic conditions.

Fig. S5 Impacts of the inhibitors of mitochondrial respiratory complexes (I, III, IV), ATP synthase and AOX on respiratory (R_d) and photosynthetic gross oxygen evolution (E_O) rates for *Euglena gracilis* cultivated in mixotrophic and photoautotrophic conditions.

Fig. S6 (a) End of exponential phase of batch cultures of *Euglena gracilis* cultivated in mixotrophic (TAP) and photoautotrophic (TMP) conditions, and in the presence of rotenone (Rot, 100 μ M) or antimycin A (AA, 10 μ M).

Fig. S7 Transmission electron micrographs illustrating subcellular organization of *Euglena gracilis* cultured in mixotrophy, photoautotrophy and photoautotrophy + 5% CO₂.

Fig. S8 Relationship between PSI relative electron transport rate and PSI + PSII photochemical rate, and relationship between PSII relative electron transport rate and E_O in *Euglena gracilis* cultivated in mixotrophic and photoautotrophic conditions.

Method S1 Detailed procedure of the proteomics analysis.

Table S1 Table containing the 544 proteins identified in *Euglena gracilis*, including several enzymes involved in the central carbon metabolism pathways.

Table S2 Table containing 112 proteins showing significant log₂-fold increase or decrease (in ratio of normalized protein abundance) depending on the trophic state in *Euglena gracilis*.

Please note: Wiley Blackwell are not responsible for the content or functionality of any Supporting Information supplied by the authors. Any queries (other than missing material) should be directed to the *New Phytologist* Central Office.



About *New Phytologist*

- *New Phytologist* is an electronic (online-only) journal owned by the New Phytologist Foundation, a **not-for-profit organization** dedicated to the promotion of plant science, facilitating projects from symposia to free access for our Tansley reviews and Tansley insights.
- Regular papers, Letters, Viewpoints, Research reviews, Rapid reports and both Modelling/Theory and Methods papers are encouraged. We are committed to rapid processing, from online submission through to publication 'as ready' via *Early View* – our average time to decision is <26 days. There are **no page or colour charges** and a PDF version will be provided for each article.
- The journal is available online at Wiley Online Library. Visit www.newphytologist.com to search the articles and register for table of contents email alerts.
- If you have any questions, do get in touch with Central Office (np-centraloffice@lancaster.ac.uk) or, if it is more convenient, our USA Office (np-usaoffice@lancaster.ac.uk)
- For submission instructions, subscription and all the latest information visit www.newphytologist.com